Towards Kilometric Distance Measurements with Air Refractive Index Compensation

J. Guillory, J-P. Wallerand, D. Truong
Laboratoire Commun de Métrologie LNE-Cnam,
LNE, 1 rue Gaston Boissier, 75015 Paris, France

R. Šmíd
Institute of Scientific Instruments of the CAS, v.v.i.
Královopolská 147, 612 64 Brno, Czech Republic

C. Alexandre,
Centre d'Études et de Recherche en Informatique et Communications (CEDRIC),
Cnam, 292 rue St-Martin, 75003 Paris, France

Abstract. The accuracy of kilometric-range distance measurements by electro-optical instruments is still limited by the determination of the air refractive index along the measurement path. Thus, a sub-millimetric accuracy is not reachable with classical instruments for such distances. However, a two-wavelength approach offers a promising route towards a compensation of air index fluctuations, and so towards more accuracy. In this paper, the principle of the two-wavelength absolute distance meter is explained, an experimental setup working at 785 nm and 1550 nm is described, and the first experimental results are presented.

Keywords. Kilometric distance, optical telemetry, two-wavelength telemetry, absolute distance meter.

1 Introduction

Absolute long-distance telemeters are of great interest for large scale surveying applications. A telling example is the field surveys that have been carried out before the construction of the Large Hadron Collider (LHC) at CERN [Gervaise (1983)]. In that case, the instrument used was a two-wavelength absolute distance meter called Terrameter. The latter, marketed in very small quantities, was able to compensate the air index fluctuations [Earnshaw (1972)] [Slater (1976)] using the knowledge of the air index dispersion. Today, it is no more in operation because of its quite difficult use and its complex maintenance process that required specific skills. However, the geodetic research, and even the classical surveys, could take great advantage of this kind of instrument that enables high accuracy optical distance measurements.

Currently, for long-range outdoor applications, the best state-of-the-art commercial measurement devices claim an uncertainty of 1.6 mm up to 1 km. In the past, the Mekometer ME5000 from the former Kern company offered a resolution of 100 µm. Even if it has not been manufactured for many years, this instrument is still used by several geodetic institutes. These uncertainties might be considered to be sufficient, but they do not take into account the atmospheric parameters. The operator has to estimate himself the air refractive index, typically using the Edlén formula [Edlén (1966)], then to correct the distance measurements realized by his instrument. In such a case, the temperature of the air travelled by the optical beam is the most critical measurand: to achieve a resolution of 100 µm over 1 km, the temperature has to be known at ±0.1 °C along the optical path. To reach this relative uncertainty of 10^{-7}, a two-wavelength approach, as already experienced in the 1970s, can be the solution. However, up-to-date technologies have to be adopted: fiber-optic components can be used to obtain a compact and robust system that would not require optical alignment, and digital electronics can be implemented to provide an efficient signal processing with a user friendly operation.

To be able to compensate the air index fluctuations, a two-wavelength system measures the same path with two different wavelengths, and then takes advantage of the knowledge of the air index dispersion between near infrared and visible lights. Indeed, the distance measured for a given wavelength and an air refractive index equal to one is simply corrected by the product of a factor depending only of the air indexes n and the difference between both measurements, $D_{\lambda 1,\, n=1}$ and $D_{\lambda 2,\, n=1}$:

$$distance = D_{\lambda_1,n=1} - \frac{n(\lambda_1,t,p,x,p_\omega)-1}{n(\lambda_2,t,p,x,p_\omega)-n(\lambda_1,t,p,x,p_\omega)} \times \left(D_{\lambda_2,n=1} - D_{\lambda_1,n=1}\right) \quad (1)$$

To deduce the true distance travelled by light, the term $n(\lambda_1)-1 \,/\, n(\lambda_2)-n(\lambda_1)$, called factor *A*, has to be determined. According to Bönsch and Potulski [Bönsch (1998)], the air refractive index *n* can be written in the following form (updated Edlén equation):

$$n(\lambda,t,p,x,p_\omega)-1 = K(\lambda)\cdot D(t,p,x) - p_\omega \cdot g(\lambda) \quad (2)$$

with *K* and *g* two factors described in [Bönsch (1998)] and depending only on the wavelength λ, and *D* a factor also described in [Bönsch (1998)] and depending on the temperature *t*, the total pressure *p* and the CO_2 content *x*. As shown in Formula (2), the air refractive index also depends on the partial pressure of water vapor p_ω.

The factor *A* can be simplified for dry air ($p_\omega = 0$): in that case the distance depends only on the distance measurements at both wavelengths with $n = 1$ and on the factors *K* (i.e. the wavelength values). More generally, in moist air, the factor *A* can also be calculated if a reliable estimate of p_ω (no critical measurand) can be made. And finally, the corrected distance takes the following form [Meiners-Hagen (2008)]:

$$distance = \frac{k(\lambda_1)D_{\lambda_2,n=1} - k(\lambda_2)D_{\lambda_1,n=1}}{k(\lambda_1)-k(\lambda_2)+p_\omega\, g(\lambda_1)k(\lambda_2)-g(\lambda_2)k(\lambda_1)} \quad (3)$$

We are currently developing such an instrument able to compensate the air index fluctuations. It is based on the couple of wavelengths 785 nm and 1550 nm where on-the-shelf fiber-optic components can be found, including laser diodes, intensity modulators and optical amplifiers. Finally, if we are able to determine each measurement distance with an accuracy better than 20 µm, then the temperature compensated distance will be known with a sub-millimetric accuracy, i.e. 50 times degraded due to the factor *A*.

2 Experimental Setup

2.1 Two-wavelength Design

The complete setup of the developed two-wavelength telemeter is depicted in Figure 1.

The distances $D_{\lambda1,\,n=1}$ and $D_{\lambda2,\,n=1}$ are measured from the phases accumulated by Radio Frequency (RF) sine waves propagated in air, one carried by a laser beam at 785 nm (in red in Fig. 1), and another one by a laser beam at 1550 nm (in yellow in Fig. 1). These laser beams are intensity-modulated at 4261 MHz, while phases are calculated from the difference between a sine wave propagated in free-space, reflected on a target and finally detected by a

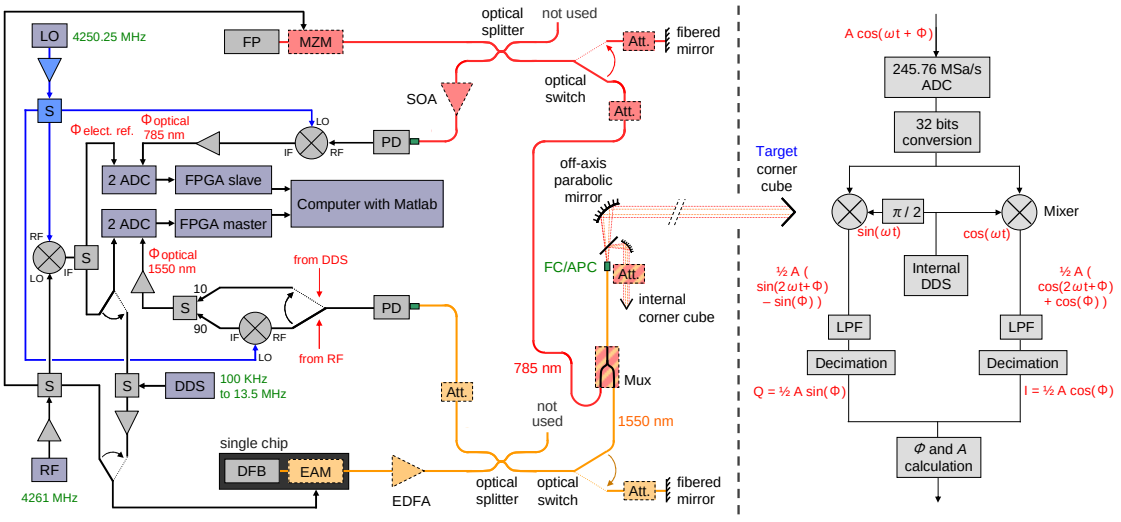

Fig. 1 Functional diagram of the two-wavelength telemeter on the left and Signal processing inside the FPGA for a given input RF signal on the right.

photodetector ($\phi_{optical\ measure}$) and another sine wave coming directly from the RF synthesizer ($\phi_{electrical\ reference}$). The distances D are so equal to:

$$2\times D_{\lambda,n=1} = \left(\frac{\phi_\lambda}{2\pi} + k\right)\times \Lambda_{n=1} \qquad (4)$$

with:

$$\Lambda = \frac{c}{n\cdot f_{RF}} \quad \text{and} \quad \phi_\lambda = \phi_{opt.\,meas.} - \phi_{elect.\,ref.} \qquad (5)$$

where ϕ_λ is the measured phase shift, c the speed of light in vacuum, n the group refractive index of air, f_{RF} the frequency modulation, and k an integer number corresponding to the number of synthetic wavelengths Λ within the distance to be measured. This integer k is determined at one wavelength only by a set of measurements at different RF carriers. Indeed, RF switches have been implemented in the system to allow, on request, a Direct Digital Synthesizer (DDS) to modulate the 1550 nm laser beam with low frequencies from 100 kHz to 13.5 MHz.

A Fabry–Pérot (FP) and a Distributed FeedBack (DFB) laser diodes, temperature controlled by Peltier elements, emit the stabilized wavelengths at 785 nm and 1550 nm, respectively. Each of these fiber-guided laser beams is then externally intensity-modulated, using a Mach-Zehnder Modulator (MZM) at 785 nm and an Electro-Absorption Modulator (EAM) at 1550 nm. After passing through 2x2 non polarization-maintaining fiber-optic splitters that play the role of circulators, the two optical beams are mixed together using an off-the-shelf Wavelength Division Multiplexer (WDM): the input lights, from a 780 nm and 1550 nm Single Mode Fiber (SMF), are combined into a single 780 nm SMF. However, due to bad propagation of the 1550 nm laser beam in the 780 nm SMF, we have changed the common fiber to a 1550 nm SMF.

At this fiber output, the two optical beams are emitted in free space. As shown in Figure 2 (on the left), we have designed our own optical head. We have chosen a 90° off-axis parabolic mirror to collimate the optical beams over a long distance. Thus the setup is achromatic and can be used indifferently at 635 nm (visible laser for alignment purpose), 785 nm or 1550 nm. This mirror – of 51 mm of diameter – is placed at 152.4 mm from the fiber termination, which provided spot sizes (at 1 % power level) of 43 and 48 mm at 785 and 1550 nm, respectively, due to fiber numerical apertures of 0.138 and 0.152 (value determined experimentally).

After long distance propagation and reflection on the target, the two beams are reinjected in the same fiber as the one used for emission, then separated by the WDM. At the output, and after passing through the 2x2 optical splitters, the two laser beams are directed towards their respective photodiode, a Gallium Arsenide (GaAs) Metal-Semiconductor-Metal (MSM) photodiode at 785 nm (reference G4176 from Hamamatsu), and an Indium Gallium Arsenide (InGaAs) Positive-Intrinsic-Negative (PIN) photodiode at 1550 nm (reference EM169-03 from EM4).

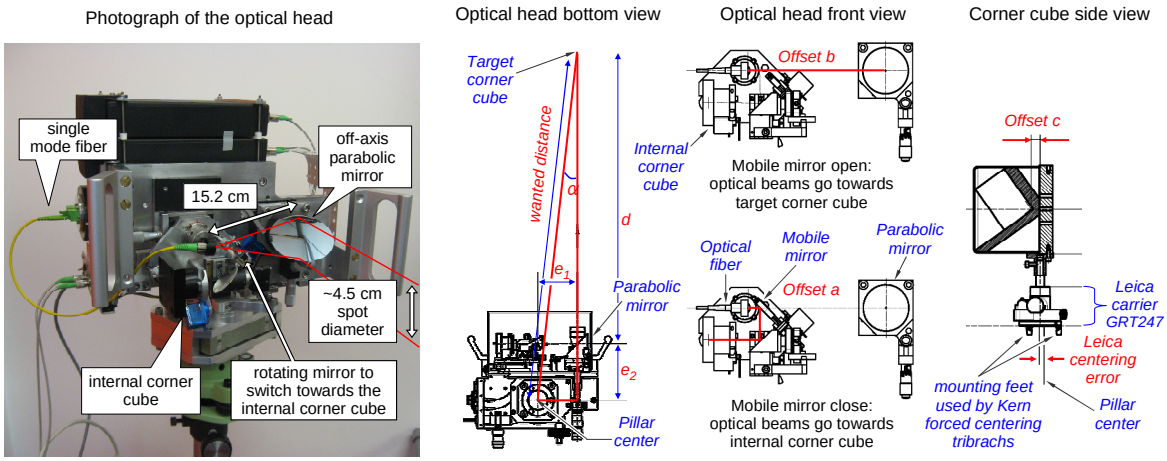

Fig. 2 Photograph of the optical head on the left and Drawing of the different offsets on the right.

As free-space propagation and optical reinjection induces important optical losses (at least 9 dB) and large intensity variations, optical amplification stages are required. At 785 nm, a Semiconductor Optical Amplifier (SOA) has been inserted just before the photodiode to take advantage of its high gain without saturate it, while at 1550 nm, an Erbium-Doped Fiber Amplifier (EDFA) has been inserted just after the intensity modulator to amplify the stable optical power coming from the laser and so minimize noise.
After photodetection, signals are down-converted by a Local Oscillator (LO) into an Intermediate Frequency (IF) of 10.75 MHz before RF amplifications. This approach has two advantages: first, the system is less sensitive to the amplitude to phase coupling (AM/PM) occurring in the electronic stages, and secondly, this reduces the bandwidth required by the phasemeter.

2.2 Phasemeter Operation

A phasemeter based on Field Programmable Gate Arrays (FPGA) has been designed for high accuracy phase measurements. A first FPGA called "master" deals with the first wavelength, at 1550 nm, and measures the phases and the amplitudes of two input RF signals: electrical reference and optical measure. A second FPGA with the same design and called "slave" performs the same measurements for the second wavelength, at 785 nm. These two systems are completely independent; nevertheless their measurements are synchronized, and locked on the same 10 MHz oven controlled quartz oscillator.
For each FPGA, the input signals are captured by a daughter card using 14 bit and 245.76 MSa/s Analog to Digital Converters (ADC). They are then processed by the FPGA. They are first transposed to baseband using digital down-converters as shown in Figure 1 (on the right). These down-conversions consist in splitting the RF input signal into two paths and mixing each of them with an internal DDS operating at the measurement intermediate frequency. The amounts thus obtained correspond to the sum and difference frequencies. Lowpass filters reject the sum frequencies to keep only the DC components: an in-phase signal I and a quadrature signal Q as one of the local oscillators was 90° phase shift. At this step the data are decimated to a lower sampling rate to minimize the computation time. Note that the filtering operation and the decimation present a linear phase with an impulse response optimized so that the total lag is as short as possible, and with a frequency response approaching a rectangular shape. The aim is to realize stable and accurate measurements as fast as possible.
Lastly the phasemeter electronic performs the phase and amplitude measurements of the input signal.

$$\begin{aligned} \phi &= arctan(Q/I) \\ A &= 2 \cdot \sqrt{I^2 + Q^2} \end{aligned} \qquad (6)$$

To this end, a COordinate Rotation DIgital Computer (CORDIC) has been implemented to calculate the trigonometric functions.
The measurement time will depend on the filling time of the lowpass filters and of the decimation factors. In our case, the filters are loaded in 10 ms and data are decimated by a factor 10^5, which imposes new results at the phasemeter output every 400 µs. To avoid filter loading between each measurement, we work by block of 50 measurements. Thus, after having filled the filters, the results are available to the rhythm of the output sampling rate.
A micro-controller integrated in the FPGA carries out the data transfer to Matlab. The amplitudes and phases information coded on 32 bits are sent using a serial communication.
Last but not least, a debug card has been added to the master FPGA in order to control from Matlab variable optical attenuators, optical and electrical switches, a mobile mirror, and the external DDS used for the determination of the number of synthetic wavelengths within the distance to measure.

2.3 Distance measurement

Temperature changes in the optoelectronic and microwave components, but also mechanical stresses on optical fibers, can induce drifts on the phase measurement, and so on the measured distance. To compensate these variations, we periodically perform a "zero measurement" with a reference distance supposed to be fixed. Thus, all variations observed on this link will be interpreted as drifts coming from the system and so removed from the measured distance. In practice, this solution has been implemented in two stages.

For the short-term distance variations, high-speed zero measurements are carried out every 250 ms thanks to optical switches based on Micro-Electro-Mechanical Systems (MEMS) and to fiber-optic reference links of a few centimeters. The drawback of this solution is that the optical switches are not wideband. Thus, each wavelength has its own reference path, which is not so close to the fiber termination due to the wavelength multiplexer. Finally distance variations can still be observed, but the latter evolve slowly, over period of minutes or day-to-day.

For the medium/long-term drifts, a mechanical zero, common to both wavelengths, is performed. Indeed, thanks to a motorized mobile mirror, the free-space laser beams are deviated at the beginning of each distance measurement towards a small reference corner cube. This corner cube, called internal, is mounted on the optical head as shown in Figure 2.

Thus the final distance is measured in the following manner:

$$D = \left(D_{measure\ pa\ th} - D_{reference\ \ path}\right)_{internal\ \ corner\ \ cube} - \left(D_{measure\ pa\ th} - D_{reference\ \ path}\right)_{target\ \ corner\ \ cube} \quad (7)$$

A proper distance measurement also requires that the different instrument offsets have been taken into account. Indeed, when the optical head is mounted on a pillar, its center does not match with the mechanical zero of our system. To obtain the wanted result, we have first to consider the offset due to the bad centering of the parabolic mirror (Fig. 2, drawing on the left), then to subtract the offsets due to the distance difference between the internal corner cube and the parabolic mirror (Fig. 2, drawings in the center). Lastly, the offset of the target corner cube has also to be considered (Fig. 2, drawing on the right).

Therefore, the wanted distance (i.e. Pillar center to Target corner cube center) is calculated as follows:

$$\alpha = atan\left(e_1 / \left(e_2 + d\right)\right) \quad (8)$$

with:

$$wanted\ \ distance\ = e_1 / sin\left(\alpha\right) \quad (9)$$

The distance between the parabolic mirror and the target corner cube, *d*, is determined from the measured distance. Thus:

$$wanted\ distance\ = \sqrt{e_1^{\ 2} + \left(e_2 + measured\ \ distance + a - b + c\right)^2} \quad (10)$$

Last precaution, we have to place the parabolic mirror of the optical head and the center of the target corner cube at the same height to avoid additional errors.

3 Experimental Results

3.1 Comparison to the 600 m long PTB reference baseline at 1550 nm.

The two-wavelength system has been realized step by step, i.e. one wavelength after another. Thus, in a first time, the system worked at only one wavelength, 1550 nm. From Fall 2014 to Spring 2015, this one-wavelength system was characterized, in particular in term of resolution, with indoor and outdoor measurements [Guillory (2014)] [Guillory (2015)]. Among other things, the system has been tested outdoor, for distances up to 1.2 km. A resolution of 15 µm was demonstrated, during a calm day, with a cloudy sky and a temperature around 12 °C [Guillory (2016)].

In summer 2015, in order to evaluate the accuracy of this one-wavelength system, a comparison has been carried out over the 600 m long baseline of the Physikalisch Technische Bundesanstalt (PTB) located in Braunschweig (Germany). This baseline consists of eight pillars aligned in a straight line, which allows us to measure 28 different inter-pillar distances. Their positions, relatively to the first pillar, are approximately 50, 100, 150, 250, 350, 500 and 600 m.

The exact inter-pillar distances have been determined between the 7th and the 10th July 2014 by the Finnish Geodetic Institute (FGI) using a Mekometer ME5000. This instrument serves as a transfer standard to calibrate a large number of high-precision baselines across the world from the 864 m long FGI baseline at Nummela (Finland), a baseline well established for decades. FGI certifies expanded uncertainties over the inter-pillar distances between 150 µm for short distances (50 m) and 460 µm for long distances (600 m).

The PTB baseline is completed with weather sensors installed along it: 60 Pt-100 temperature sensors placed every 10 m from 5 to 595 m, 2 pressure gauges placed at 150 and 450 m, and 6 humidity sensors placed every 50 m from 50 to 550 m. Thus,

we can estimate the value of the air refractive index between two pillars. Note that the weather sensor values are updated every 30 s.

Our system has so been compared to the PTB reference baseline using the 28 inter-pillar distances. This was done from the 29th June to the 3rd July 2015, a perfectly sunny week, with temperatures up to 28°C. The baseline, bordered on one side by a forest and on another side by a screen wall, was protected from wind.

The distance measurement procedure consisted in recording 16200 distance measurements within a period of two and a half minutes, selecting the values with an acceptable power level [Guillory (2015)] [Guillory (2016)], and calculating the final result as the average of these values. This procedure was repeated several hundred of times during a full week, without any problem, which demonstrates the robustness of the developed telemeter.

On the whole set of measurements we have performed, in more than 95 % of the cases, the standard deviation over a short period of 15 s, i.e. 1800 recorded values, is lower than 24 µm. This value at short-term, i.e. with relatively constant atmospheric parameters, shows us the instrument resolution.

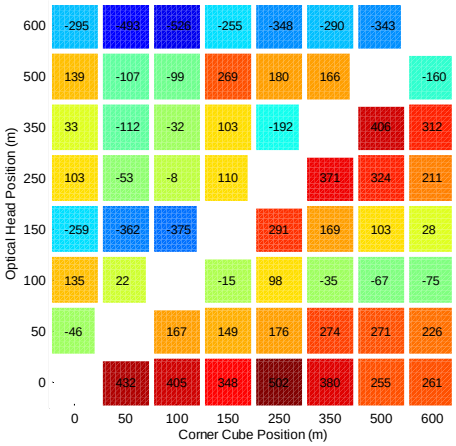

Fig. 3 Error in µm as a function of the optical head and target corner cube positions. The cold colours represent the negative errors while the warm colours represent the positive errors.

The instrument accuracy was obtained comparing the 28 inter-pillar distances to the FGI measurements. The results obtained with our one-wavelength system at 1550 nm and the air index calculated from the PTB weather sensors are depicted in Figure 3.

A pattern emerges from this figure: the upper left triangle (when the optical head position is lower than corner cube position) is constituted with a majority of negative errors while the lower right triangle (when the optical head position is higher than the corner cube position) is constituted with a majority of positive errors.

The causes of this pattern are difficult to identify. Nevertheless, a large part can probably be attributed to mechanical offsets. In particular, we have not considered the centring error of the Leica carriers GRT247 we use to mount the optical head and the target corner cube on the Kern forced centering tribrachs of each pillar (see Figure 2). According to the manufacturer datasheet, the centring accuracy equal to 1 mm. In practice, we have measured afterwards in our labs centering errors up to 355 µm. The latter induce systematic errors proportional to the sine of the angle between the Kern forced centering tribrachs and the Leica carriers GRT247, and as we did not take into account this angle value during the PTB measurements, an uncertainty of ±355/sqrt(2) µm (k = 1) has to be considered (arc sine distribution [BIPM (2008)]).

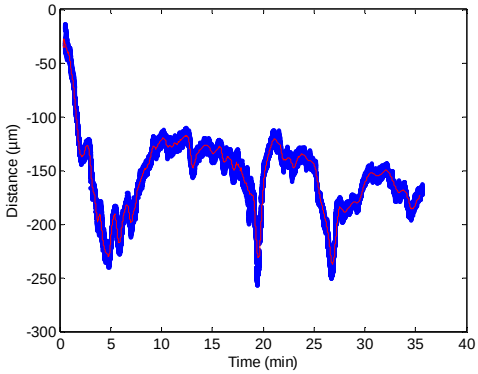

Fig. 4 In blue, variations as a function of time for the optical head placed on pillar 0 m and the target on pillar 350 m. The red curve represents the moving average over two and a half minutes.

Additionally, after carrying out long-term measurements between 15 and 60 min, we have observed important distance variations as a function of the time. Figure 4 shows an example of these variations for the optical head placed on pillar 0 m and the target corner cube on pillar 350 m. Thus, different results can so be obtained, depending on the moment when the two and a half minute long measurements are performed. Figure 5 summarizes the peak-to-peak variations as a function of the

measured distance: a quasi-linear rise of 0.7 µm/m can be observed. Investigations are under progress to understand this phenomenon. However, these drifts, with a fairly random distribution shape, has also to be taken into account: by opting for a rectangular distribution with a width *w* as defined by Figure 5, the uncertainty is ±0.7/sqrt(12) µm/m (k = 1) [BIPM (2008)].

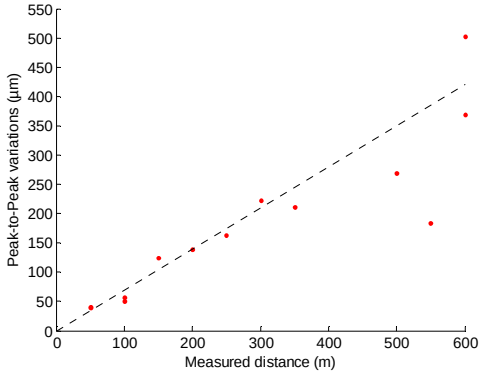

Fig. 5 Peak-to-peak variations as a function of the measured distance (in blue) and the linear regression of 0.7 µm/m (in black).

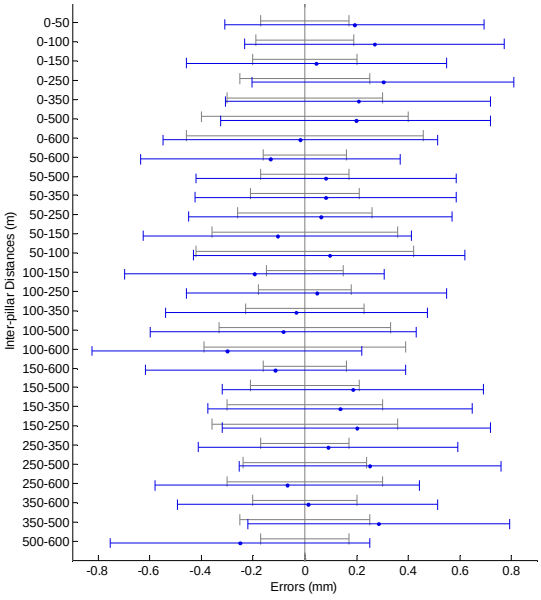

Fig. 6 The error as a function of the average inter-pillar distance: our results (in blue) and the expanded uncertainties of the PTB baseline as certified by FGI (in grey).

The Leica centering error and the distance drifts proportional to the measured distance are the two main sources of errors. At a lower level, we consider also an uncertainty due to temperature sensors (±0.1 µm/m for a temperature known at ±80 mK) and pressure sensors (±0.1 µm/m for a pressure differences between the two sensors up to 25 Pa).
Finally, to follow what was done by FGI, we give only one inter-pillar value: it is equal to the average between two measurements, from the optical head position located on pillar X to the target corner cube located on pillar Y, and inversely. Figure 6 compares our results to the FGI ones taking into account the error bars for k = 2

3.2 Comparison to the 3 m-long LNE interferometric bench at 785 and 1550 nm.

The two-wavelength system was finalized in Fall 2015. To evaluate its accuracy, a comparison to the 3 m long interferometric bench of the Laboratoire National de métrologie et d'Éssais (LNE) has been carried out. Similarly to the measurements on the PTB baseline, we have measured the distances using a weather station to estimate the air refractive index. The results are presented in Figure 7: the standard deviation on the error equal to 6.3 µm at 785 nm and 1.6 µm at 1550 nm.

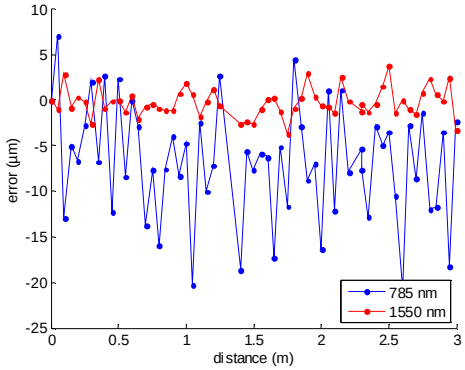

Fig. 7 Error as a function of the interferometer distance, at 785 nm in blue and at 1550 nm in red.

With this two-wavelength system, we can perform a distance measurement with air refractive index compensation. Thus, we applied the Formula 3 corresponding to moist air using the measurements of Figure 7. In that case, the factor *A* is calculated from both wavelengths λ_1, λ_2 and the partial pressure of vapour p_ω only. The latter, between 851 Pa and 866 Pa, is provided by the weather station. We finally obtain the Figure 8 with a standard deviation of 323 µm, i.e. 50 times more due to the factor *A*, as expected.
At the present time, the accuracy is progressively deteriorated when the optical losses in free-space

propagation increase. Indeed, the system accuracy is currently limited by different optical crosstalks, means unwanted signals that are modulated at the same frequency as the useful signal and that add to it. These crosstalks, coming from reflections at optical fibre connections, induce a sinusoidal error depending on the signal to crosstalk ratio. Thus, we are working hard to remove all the crosstalk.

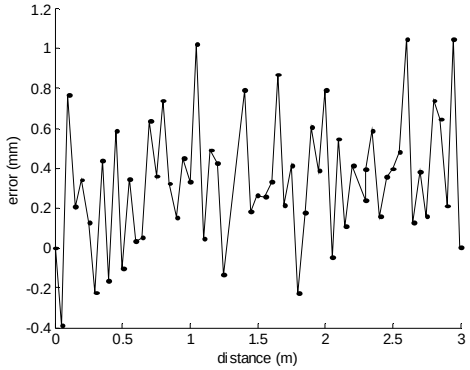

Fig. 8 Error with air refractive index compensation for the two-wavelength system as a function of the interferometer distance.

4 Conclusion

We have designed a robust, compact, and so transportable, two-wavelength telemeter. Until now, it has been tested over 3 m and it presents an accuracy of 646 µm (k = 2). Next step will consist in validating these performances over greater distances. Indeed, comparisons to the 50 m long interferometric bench of the Polish metrology institute is planned in February 2016 and to the 864 m long FGI reference baseline during Spring 2016.
The comparison carried out at one wavelength at the PTB baseline up to 600 m have helped us to identify the limitation of our system for longer distances. Therefore, we are currently improving our system. Among other things, a new optical head with reduced offsets is being designed; in particular the optical beams will pass by the pillar center to have an instrument offset independent of the measured distance.

Acknowledgement

This work was partly funded by the European Metrology research Program as JRPs SIB60 Surveying (http://www.ptb.de/emrp/sib60-home.html) and IND53 Luminar (http://projects.npl.co.uk/luminar). The EMRP is jointly funded by the EMRP participating countries within EURAMET and the European Union.

References

Bureau International des Poids et Mesures (BIPM) (2008). Evaluation of measurement data - Supplement 1 to the 'Guide to the expression of uncertainty in measurement" - Propagation of distributions using a Monte Carlo method'. In: *http://www.bipm.org/utils/common/documents/jcgm/JCGM_101_2008_E.pdf accessed 22nd January 2016.*

Bönsch, G. and E. Potulski (1998). Measurement of the refractive index of air and comparison with modified Edlén's formulae. *IOP Metrologia*, Vol. 35, No. 2, pp. 133-139.

Earnshaw, K.B. and E.N. Hernandez (1972). Two-Laser Optical Distance-Measuring Instrument that Corrects for the Atmospheric Index of Refraction. *OSA Applied Optics*, Vol. 11, No. 4, pp. 749-754.

Edlén, B. (1966). The Refractive Index of Air. *IOP Metrologia*, Vol. 2, No. 2, pp. 71-80.

Gervaise, J. (1983). First results of the geodetic measurements carried out with the Terrameter, two-wavelength electronic distance measurement instrument. In: *Proc. Of Geodätischen Seminar über Electrooptische Präzisionsstreckenmessung*, Munich, Germany, pp. 213-229.

Guillory, J., J-P. Wallerand, A-F. Obaton and C. Alexandre (2014). Laser diodes based Absolute Distance Meter. In: *Proc. Of. Conference on Precision Electromagnetic Measurements (CPEM)*, Rio de Janeiro, Brazil, August 24-29, pp. 490-491.

Guillory, J., J. García-Márquez, C. Alexandre, D. Truong and J-P. Wallerand (2015). Characterization and reduction of the amplitude-to-phase conversion effects in telemetry. *IOP Measurement Science and Technology*, Vol. 26, No. 8, 084006.

Guillory, J., R. Šmíd, J. García-Márquez, D. Truong, C. Alexandre, J-P. Wallerand (2016). High resolution kilometric range optical telemetry in air by Radio Frequency phase measurement. Submitted to: *AIP Review of Scientific Instruments*.

Meiners-Hagen, K. and A. Abou-Zeid (2008). Refractive index determination in length measurement by two-colour interferometry. *IOP Measurement Science and Technology*, Vol. 19, No. 8, 084004.

Pollinger, F., T. Meyer, J. Beyer, N. R. Doloca1, W. Schellin, W. Niemeier, J. Jokela, P. Häkli, A. Abou-Zeid and K. Meiners-Hagen (2012). The upgraded PTB 600 m baseline: a high-accuracy reference for the calibration and the development of long distance measurement devices. *IOP Measurement Science and Technology*, Vol. 23, No. 9, 094018.

Slater, L.E. and G.R. Huggett (1976). A multiwavelength Distance-Measuring instrument for Geophysical Experiments. *AGU Journal of Geophysical Research*, Vol. 81, No. 35, pp. 6299-6306.